

## Cyclic Behavior of Laterally Loaded Concrete Piles Embedded into Cohesive Soil

Rabin Tuladhar\*, Takeshi Maki, and Hiroshi Mutsuyoshi

*Graduate School of Civil and Environmental Engineering, Saitama University, Saitama, Japan*

### SUMMARY

Modern seismic design codes stipulate that the response analysis should be conducted by considering the complete structural system including superstructure, foundation, and ground. However, for the development of seismic response analysis method for a complete structural system, it is first imperative to clarify the behavior of the soil and piles during earthquakes. In this study, full-scale monotonic and reversed cyclic lateral loading tests were carried out on concrete piles embedded into the ground. The test piles were hollow, precast, prestressed concrete piles with an outer diameter of 300 mm and a thickness of 60 mm. The test piles were 26 m long. Three-dimensional finite element analysis was then performed to study the behavior of the experimental specimens analytically. The study revealed that the lateral load carrying capacity of the piles degrades when subjected to cyclic loading compared to monotonic loading. The effect of the use of an interface element between the soil and pile surface in the analysis was also investigated. With proper consideration of the constitutive models of soil and pile, an interface element between the pile surface and the soil, and the degradation of soil stiffness under cyclic loading, a three-dimensional analysis was found to simulate well the actual behavior of pile and soil.

**KEYWORDS:** Concrete pile, lateral loading, pile-soil interaction, seismic behavior

### 1. INTRODUCTION

Damages sustained during recent earthquakes, such as the 1995 Hyogo-ken Nanbu (Kobe) earthquake have emphasized that the seismic behavior of a structure is highly influenced not only by its superstructure, but also by the response of its foundation and the ground as well [1-3]. Hence, modern seismic design codes [4] stipulate that the response analysis should be conducted by considering the complete structural system including superstructure, foundation, and ground. In the development of a method of seismic response analysis for a complete structural system, however, it is first imperative to clarify the behavior of the soil and piles during earthquakes.

There have been a number of studies performed on small-scale piles embedded into model soil [5-7]. In small-scale models, the confining effect of the box used in the model is very significant, making these small-scale models unrealistic. Very few studies have been performed on the behavior of piles based on full-scale tests [8-10]. These studies used model soil (uniform clay or sand) and, hence, might not accurately represent the actual behavior of piles and soil.

In the consideration of the numerical analysis of pile-soil interaction, existing methods of analysis can be categorized into two groups. The more commonly used method is a simplified approach, which models surrounding soil by discrete springs and dashpots [8, 9, and 11]. These discrete models, however, do not take soil continua into account and, hence, cannot model damping and the inertial effects of soil media. Furthermore, it is difficult to properly model a soil-pile interface with these discrete methods.

With the advancement in computation capability, 3D finite element analysis has become more appealing because it can realistically model soil as a continuum media. In addition, it takes into account damping and the inertial effects of soil. Nevertheless, successful implementation of the finite element method depends on the appropriate use of various

---

\* Corresponding author: Rabin Tuladhar,  
International House 3503, Shimo-okubo 645  
Sakura-ku, Saitama-shi, Saitama 338-0825, Japan  
E-mail: rabin@mtr.civil.saitama-u.ac.jp, Fax: +81 48 858 3556, Tel: +81 80 5076 6027

parameters such as soil constitutive models, the soil-pile interface, and stiffness degradation in soil during cyclic loading. Use of the finite element method for pile-soil interaction problems is still under development. A few studies have been carried out to investigate the behavior of pile and the soil using finite element analysis [12-15]. However, these studies lack proper calibration with full-scale experimental studies.

With this in view, the main objectives of this research are to study the lateral behavior of concrete piles and soil during earthquakes using full-scale lateral loading tests and 3D finite element analysis. Full-scale monotonic and reversed cyclic lateral loading tests were performed on two instrumented concrete piles embedded into the ground. Three-dimensional finite element analysis was then performed to simulate the behavior of the experimental specimens to clarify the effects of interface element, method of piling, and degradation of soil stiffness on the response of the piles during cyclic loading.

## 2. FULL SCALE LATERAL LOADING TEST

### 2.1 Test Pile Details

The experimental program consists of a lateral loading test on two full-scale concrete piles embedded into the ground. Both test piles were hollow precast prestressed concrete piles with a diameter of 300 mm and a thickness of 60 mm. The test piles were 26 m long. Six 7-mm diameter prestressing steel bars were used for longitudinal reinforcement and spiral hoop reinforcements with a diameter of 3 mm and pitch of 100 mm were used for confining the concrete (Figure 1a). Strain gages were attached to the longitudinal reinforcements up to 12 m from the pile head, as shown in Figure 1(b).

The compressive strength of the concrete was  $f'_c = 69$  MPa and the yielding stress of the longitudinal prestressing steel was  $f_y = 1325$  MPa. The effective prestress on the concrete piles was 5 MPa.

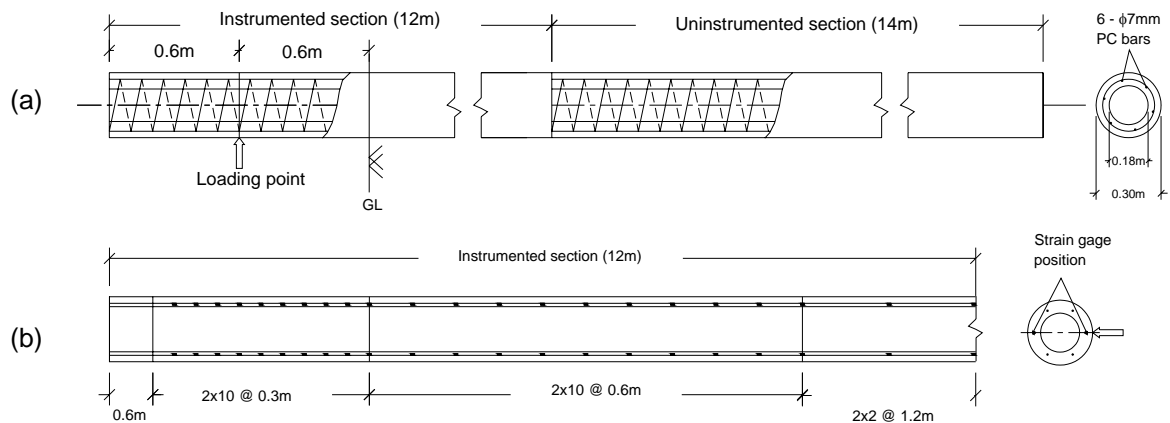


Figure 1. (a) Test pile details (b) positions of strain gages.

### 2.2 Bending Test of Pile Specimen

To investigate the mechanical properties of the test piles, a bending test was conducted on an 8-m long pile specimen with the same cross section as the test piles (Figure 2). From the bending test, yielding moment and ultimate moment of the section were obtained as  $M_y = 42$  kNm and  $M_u = 51.2$  kNm, respectively. The moment-curvature curve for the pile section is shown in Figure 3.

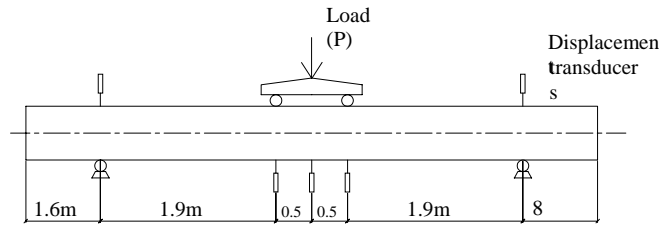


Figure 2. Bending test on pile specimen with same cross section as test piles.

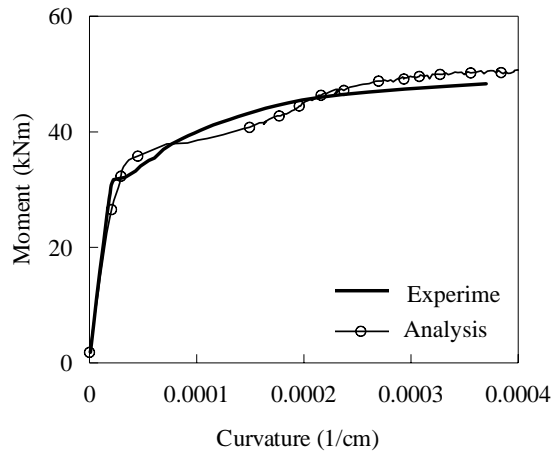


Figure 3. Moment-curvature curve of pile section from bending test.

2.3 Subsurface Investigation

A standard penetration test (SPT) was performed at the experimental site to investigate the relevant soil parameters. The SPT-N values obtained from the test are shown in Figure 4 along with soil type. The water table was 1.3 m below ground level.

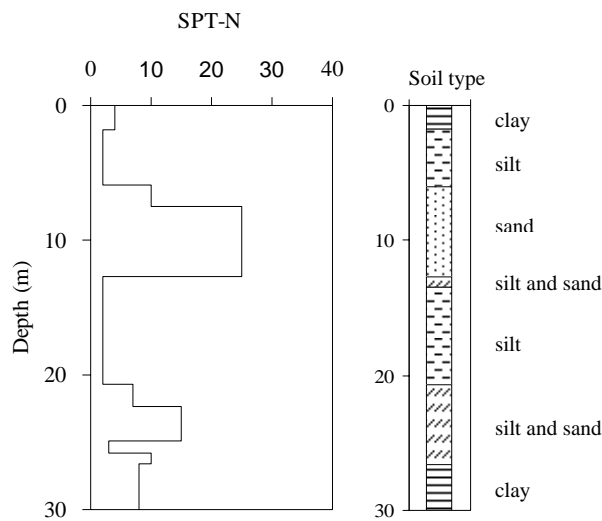


Figure 4. Soil profile at test site.

### 2.4 Experimental Setup

Piling was carried out by drilling. Drilling was done using a 450-mm diameter auger. The drilled shaft was then filled with bentonite-cement slurry to stabilize the soil and to facilitate piling. The pile was then inserted into the drilled shaft. Test piles were embedded up to 24.8 m from the ground level (GL), where a sand layer exists. The head of the pile and the loading point was 1.2 m and 0.6 m from GL, respectively. Reaction frames were set up on six reaction piles, as shown in Figure 5. The reaction piles were driven to a depth of 10 m. The experimental setup was done in accordance with JSF standards [16].

Test pile SP1 was subjected to monotonic loading, whereas test pile SP2 was subjected to reversed cyclic loading with the loading sequence shown in Figure 6. Displacement-controlled loading was applied in both cases.

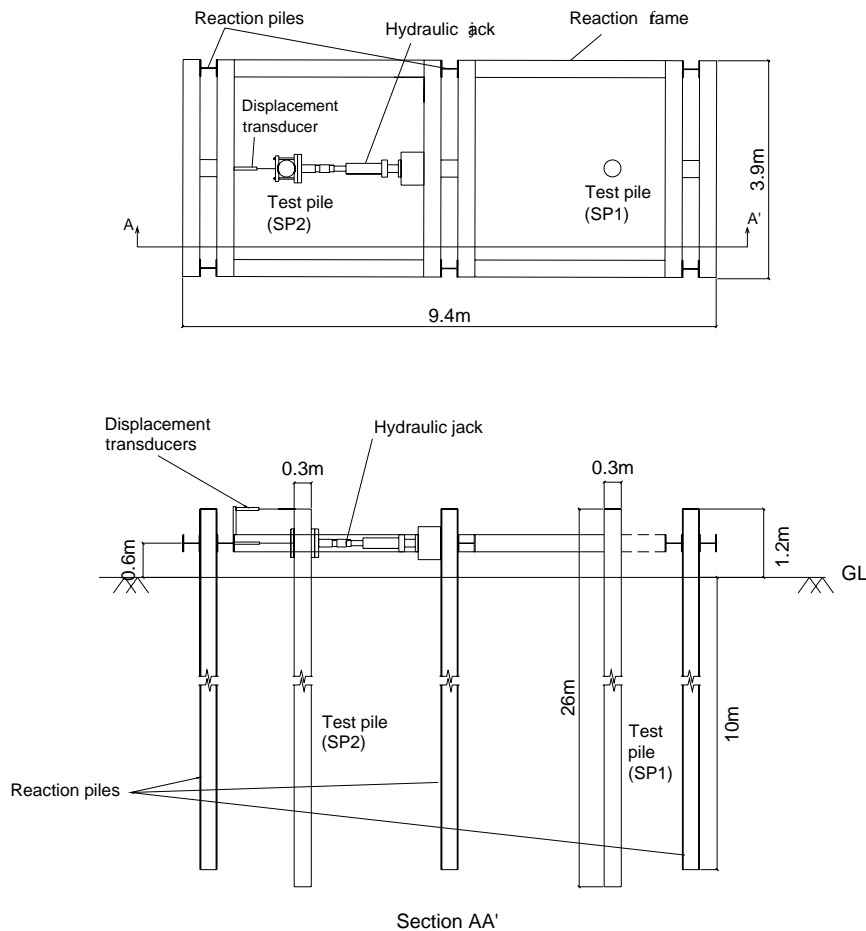


Figure 5. Experimental setup.

### 2.5 Experimental Observations

#### *Restoring Force and Deformation Relationship*

The load-displacement relationships at the loading point in the test piles, SP1 and SP2, are shown in Figure 7. In the case of monotonic loading, yielding of the pile, SP1, occurred at  $V_y = 44$  kN and the maximum lateral load carrying capacity was  $V_u = 51$  kN at the maximum displacement of 160 mm at the loading point.

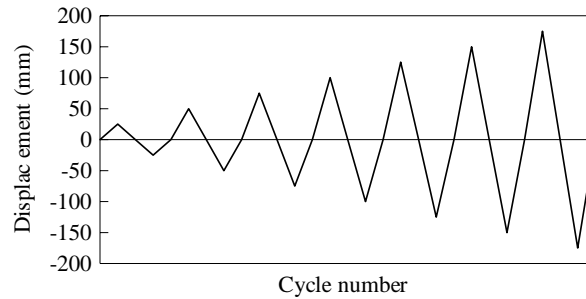


Figure 6. Loading cycle

For the specimen subjected to reversed cyclic loading, SP2, the maximum lateral load carrying capacity was 31.5 kN at the maximum displacement of 170 mm at the loading point. Compared with the monotonic loading, the lateral load carrying capacity of the pile under reversed cyclic loading had degraded significantly by 28%. The degradation in lateral load carrying capacity in reversed cyclic loading is due to the degradation in shear modulus of the soil with cyclic loading.

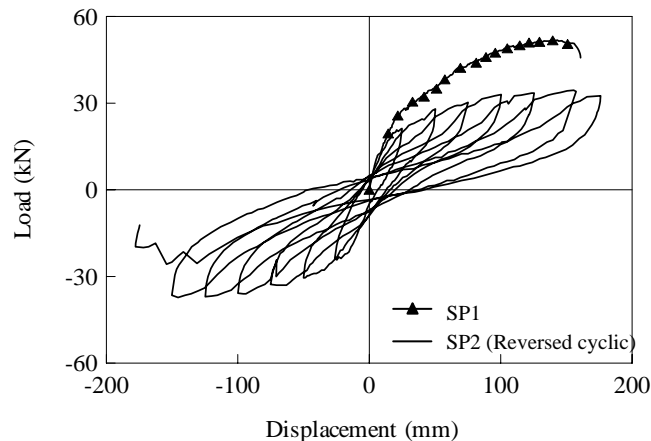


Figure 7. Load-displacement curve for monotonic test (SP1) and reversed cyclic test (SP2).

#### *Curvature Distribution and Damage Pattern*

Curvature distributions along the pile shaft were calculated from the measured strain data. The maximum curvature was attained at a depth of 0.6 m and 1.2 m from GL for specimen SP1 and SP2, respectively (Figure 8).

Flexural failure was observed in both specimens SP1 and SP2 with breaking of longitudinal reinforcement. Damage in the piles below the ground surface was examined by digging trenches around the piles after completion of the loading test (Figure 9). The maximum damage location for specimens SP1 and SP2 was at a depth of 0.6 m and 1.2 m from the GL, respectively. The deepening of the location of the plastic hinge for specimen SP2 subjected to reversed cyclic loading compared to that of specimen SP1 subjected to monotonic loading is due to the degradation of soil stiffness due to the reversed cyclic loading.

Soil deformation at ground surface around the pile for SP1 and SP2 is shown in Figure 10. In monotonic loading, a 100-mm gap was observed between the pile surface and the soil on the active (extension) side. In reversed cyclic loading, gaps of 150 mm and 170 mm were observed between the pile surface and the soil on each side of the pile.

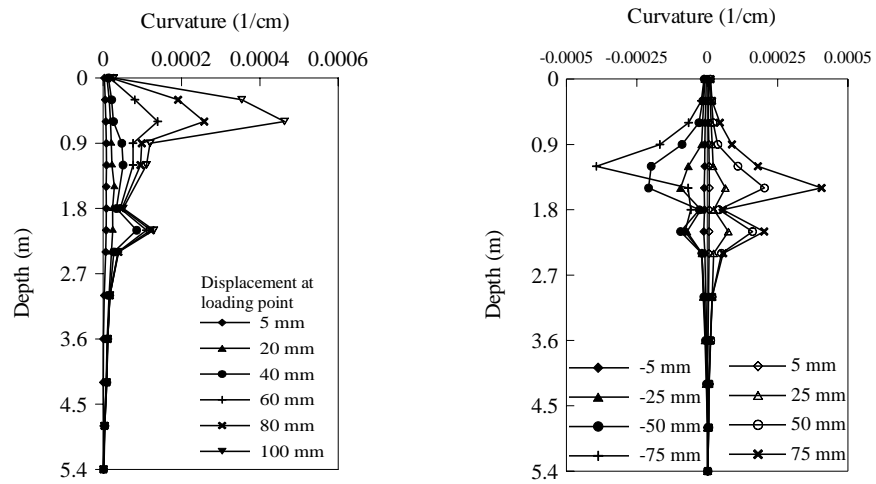


Figure 8. Distribution of curvature for (a) monotonic - SP1 and (b) reversed cyclic - SP2.

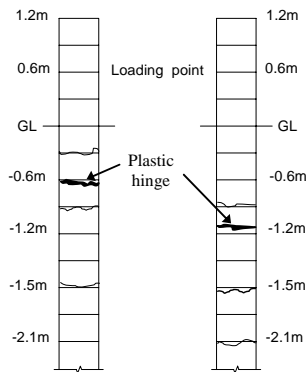


Figure 9. Damage pattern in pile (a) monotonic - SP1 and (b) reversed cyclic test - SP2.

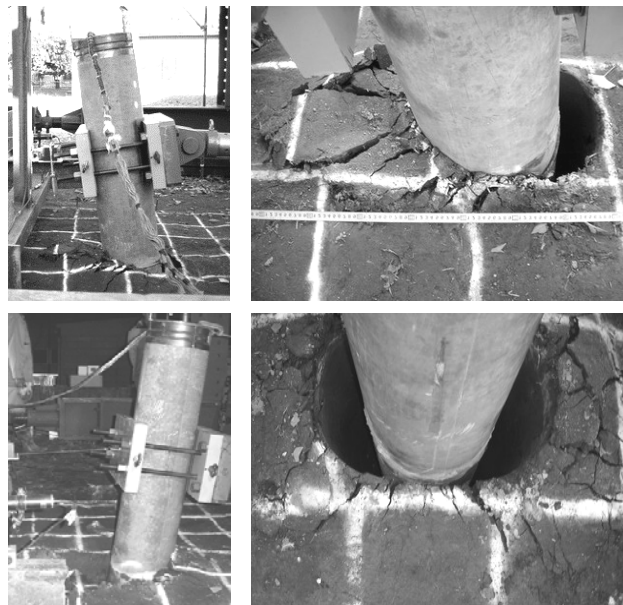


Figure 10. Soil deformation (a) monotonic - SP1 and (b) reversed cyclic test - SP2.

### 3. THREE-DIMENSIONAL FINITE ELEMENT ANALYSIS

3D finite element analysis was performed to clarify the behavior of the experimental specimens. Because of the symmetry in geometry and load, only half of the domain is considered, as shown in Figure 11. The soil and pile were modeled up to a depth of 12.5 m, a length of 6.3 m, and a width of 2.1 m. The soil properties used in the analysis are listed in Table I. Here, constant soil properties for clay and sand, as shown in Table I, were used for a depth of 0-6 m and 6-12.5 m, respectively. This assumption was made to simplify the model and to reduce computation time. However, as there is a very small amount of displacement in the pile and soil below the depth of 6 m, this assumption should not make much difference in the results. The base was fixed in all the X, Y, and Z directions. Two lateral faces of the soil model, those perpendicular to the direction of loading, were fixed in the X direction, and the remaining two lateral faces were fixed in the Y direction.

The pile and soil were modeled with 20-node isoparametric solid elements. The interface between the soil and pile surface was modeled with a 16-node interface element.

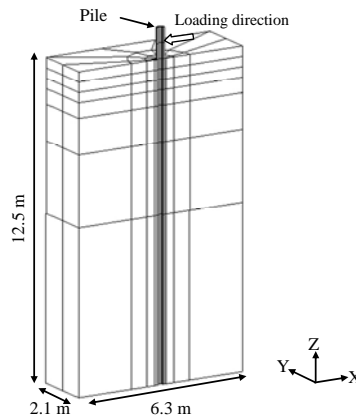


Figure 11. Finite element mesh for 3D analysis.

Table I. Soil properties used in analysis.

| Depth from GL | Soil type | Saturated unit weight (kN/m <sup>3</sup> ) | Shear strength (kPa) | Shear modulus (MPa) | Poisson's ratio ( $\nu$ ) |
|---------------|-----------|--|----------------------|---------------------|---------------------------|
| 0 – 6 m       | Clay      | 15.7                                       | 33                   | 20.4                | 0.5                       |
| 6 m – 12.5 m  | Sand      | 18.6                                       | 140                  | 154.3               | 0.5                       |

#### 3.1 Nonlinearity of concrete pile and soil

The nonlinearity of the concrete before cracking was modeled by an elasto-plastic fracture model [17]. A smeared crack model based on average stress - average strain was used to model the concrete after cracking. For the post-cracking behavior, the compression and tension model proposed by Maekawa et al. [17], as shown in Figure 12, was used. For reinforcements, the nonlinear, path-dependent constitutive model of Kato [18], as shown in Figure 12, was used. The validity of concrete pile model was tested by analyzing the bending test specimen. The moment curvature curve obtained from the experiment and the analysis of the bending test of the pile specimen are compared in Figure 3. The good agreement between the experimental and

analytical results confirms that the model used for the concrete pile can accurately simulate actual behavior.

The soil elements were separately formulated in both the deviatoric and volumetric components. The volumetric component of the soil element was taken as linear elastic. For the deviatoric component, the non-linear path dependency of soil in shear was modeled by the Ohsaki model [19], as represented by Equation (1) (Figure 13).

$$\frac{J_2'}{M} = \frac{J_2}{2G_0M} \left\{ 1 + \left( \frac{G_0}{100S_u} - 1 \right) \left| \frac{J_2}{S_uM} \right|^B \right\} \quad (1)$$

where,

$G_0$  = Initial shear modulus (N/mm<sup>2</sup>)

$J_2$  and  $J_2'$  = second invariants of deviatoric stress and strain tensors

$S_u$  = shear strength at 1% shear strain (N/mm<sup>2</sup>)

$B$  = material parameter (1.6 for sand and 1.4 for clay)

$M$  = loading parameter (1.0 when loading and 2.0 when unloading or reloading)

The material parameters of soil, initial shear modulus  $G_0$  and shear strength  $S_u$ , were calculated from the SPT-N value measured in the field by using Equations (2) and (3).

$$G_0 = 11.76 N^{0.8} \quad (\text{N/mm}^2) \quad (2)$$

$$\begin{aligned} S_u &= G_0/1100 \quad (\text{for Sand}) \quad (\text{N/mm}^2) \\ &= G_0/600 \quad (\text{for Clay}) \quad (\text{N/mm}^2) \end{aligned} \quad (3)$$

where,

$N$  = SPT-N value

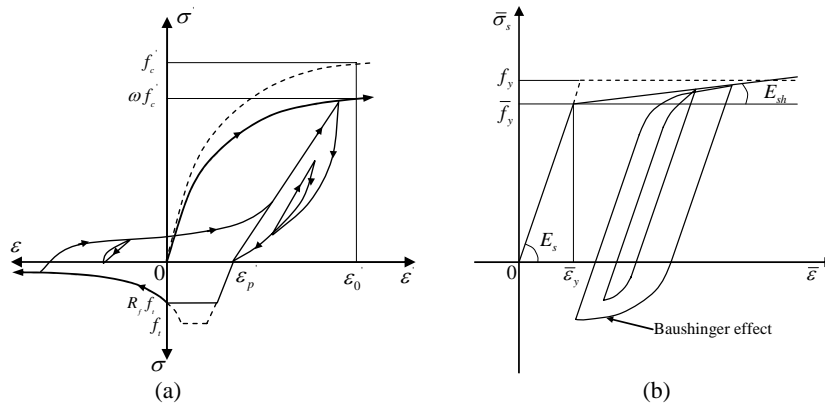


Figure 12. Nonlinear, path-dependent constitutive model for (a) concrete and (b) reinforcement.

where,

$\sigma'$  = average compressive stress;  $\varepsilon'$  = average compressive strain;  $f'_c$  = uniaxial compressive strength;  $\omega$  = strength reduction factor due to orthogonal tension;  $\varepsilon'_0$  = uniaxial strain at  $f'_c$ ;  $\varepsilon'_p$  = compressive plastic strain;  $\sigma$  = average tensile stress;  $\varepsilon$  = average tensile strain;  $f_t$  = uniaxial tensile strength;  $R_t$  = tensile strength reduction factor;  $\bar{\sigma}$  = average tensile stress;  $\bar{\varepsilon}$  = average tensile strain;  $E_s$  = initial bar stiffness;  $E_{sh}$  = stiffness of bar after yielding;  $f_y$  = yield strength;  $\bar{f}_y$  = yield strength of bar in concrete

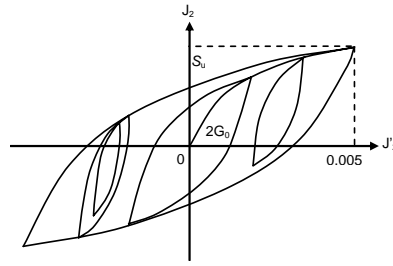


Figure 13. Nonlinear constitutive model for soil [18].

where,

$J_2$  and  $J_2'$  are second invariants of deviatoric stress and strain tensors

### 3.2 Interface element

When a pile in cohesive soil is subjected to lateral loading, the soil on the passive side (compression side) moves with the soil. However, the soil on the active side (extension side) does not move. Hence, a gap occurs between the soil and the pile surface on the active side.

To simulate this kind of opening between soil and pile surface, a 16-node interface element is used between the soil and pile surface (Figure 14). In this opening-closure model, there is no stress transfer between pile and soil during opening or tension. However, during closure or compression, a high rigidity ( $K$ ) is assumed between the pile and soil elements to avoid the overlapping of the elements during compression. In this case, no shear stress between RC and the soil element is assumed.

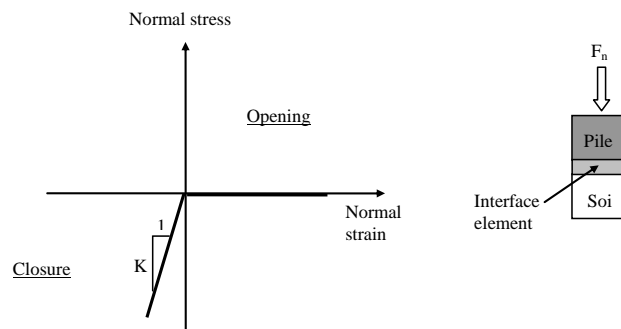


Figure 14. Opening-closure model for interface element between pile and soil.

### 3.3 Bentonite-cement layer modeling

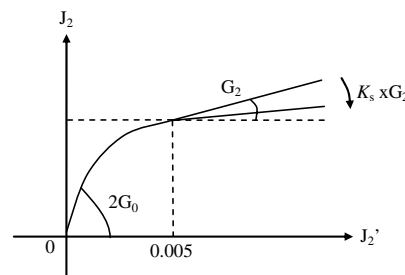
As discussed earlier, piling was carried out by drilling, which is widely used for piles having diameters smaller than 300 mm. The diameters of the test piles used in this study were 300 mm and a 450-mm auger was used for drilling. Bentonite-cement slurry was poured into the drilled shaft to stabilize the soil and to facilitate piling. Hence, the remaining 75-mm gap between the soil and the pile was filled with bentonite-cement slurry. The unit weight of the bentonite-cement was  $11.7 \text{ kN/m}^3$ . The unconfined compressive strength ( $q_u$ ) of the bentonite-cement was determined to be 19.6 kPa based on an unconfined compressive test. The shear strength ( $S_u$ ) and the initial shear modulus ( $G_0$ ) for bentonite-cement was determined to be 9.8 kPa and 5.8 MPa, respectively. Ohsaki's model [19] was also used for determining the stress-strain relationship for bentonite-cement. In the analysis, the effect of the bentonite-cement layer around the pile on the lateral capacity of the pile was also investigated.

### 3.4 Degradation of the stiffness of clay with cyclic loading

The undrained cyclic triaxial and simple shear tests on clay specimens performed by Thiers and Seed [20] and by Gerolymos and Gazetas [22] have shown that cyclic loading in cohesive soil

leads to two important effects: (i) reduction in soil modulus and (ii) reduction in undrained shear strength. Shear modulus was found to decrease by approximately 50-80% for a peak strain of 3%. The reduction in shear modulus of soil with cyclic loading leads to a reduction in the lateral load carrying capacity of the pile. This degradation in soft clay due to cyclic loading has, however, not been explicitly incorporated into the prevailing method of finite element analysis for pile-soil interaction.

In this study, the reversed cyclic loading on the pile has shown a significant reduction (28% reduction) in lateral capacity compared to the monotonic loading (Figure 7). In the current Ohsaki model used in the analysis, the deviatoric stress-strain relationship has only been tested up to 1% engineering strain level. After this strain, a constant shear modulus ( $G_2$ ) is assumed, as shown in Figure 15. To incorporate the degradation in the soil stiffness due to cyclic loading, the shear modulus after the 1% shear strain was reduced parametrically using a stiffness degradation factor ( $K_s$ ) based on the experimental results.



$K_s$  = Stiffness degradation factor

Figure 15. Incorporating stiffness degradation factor in Ohsaki soil model.

### 3.5 Analysis Parameters

In monotonic loading, three different cases were analyzed, whereas two different cases were considered for the reversed cyclic test, as shown in Table II.

Table II. 3D Finite element analysis cases.

| Loading condition | Name | Description       |                        |                            |
|-------------------|------|-------------------|------------------------|----------------------------|
|                   |      | Interface element | Bentonite-cement layer | Stiffness reduction factor |
| Monotonic         | Mon1 | No                | No                     | No                         |
|                   | Mon2 | Yes               | No                     | No                         |
|                   | Mon3 | Yes               | Yes                    | No                         |
| Reversed cyclic   | Rev1 | Yes               | Yes                    | No                         |
|                   | Rev2 | Yes               | Yes                    | Yes                        |

### 3.6 3D Finite Element Analysis Results

#### Monotonic loading

Figure 16 shows load-displacement curves obtained from 3D finite element analysis for different cases in monotonic loading. Case Mon1, which assumes a perfect bond between soil and pile, highly overestimates the lateral load carrying capacity of the pile. When a perfect bond is assumed between the soil and pile surface, soil elements on the active side (extension side) are subjected to tension. However, in reality, a gap forms between the soil and pile surface on the active side (extension side) and the soil on the active side does not contribute to the total subgrade reaction. In case Mon2, where an interface element has been considered, the load-

displacement curve has been improved and tends to agree with the experimental result. Here, separation between soil and pile occurs when the stress state at the interface shifts from compression to tension. The load-displacement curve of Case Mon2 shows an improved correlation between the experimental result compared to that of Case Mon1, however, the lateral capacity of the pile is still overestimated in case Mon2.

The effect of gap formation on the displacement of the soil in the vicinity of laterally loaded piles is shown in Figure 17. Contour lines of horizontal displacements in case Mon1 at maximum displacement at the loading point (90 mm) is shown in Figure 17(a), while Figure 17(b) shows contour lines for case Mon2 at maximum displacement at the loading point (150 mm). For case Mon1, where a perfect bond between soil and pile is assumed, soil is displaced on both the passive and active sides. However, for case Mon2, where the interface element was considered between soil and pile, soil displacement only occurred on the passive side. The deflected shape of the piles for case Mon1 and Mon2 are shown in Figure 18(a) and Fig 18(b), respectively.

In case Mon3, where the 75-mm bentonite-cement layer around the pile was also considered, the analytical results tend to correlate well with the experimental results. This shows that the disturbance caused around the soil during the drilling process has a significant effect on the lateral capacity of the piles. The curvature distribution along the pile shaft for case Mon3 is shown in Figure 19. The maximum curvature occurred at a depth of 0.6 m from GL, which correlates well with the experimental results. The zigzagging of the curvature distribution in Figure 19 was caused by the initiation of cracks. Strain values increased sharply near the cracks. The analysis could well simulate the curvature distribution at a higher strain level. However, there are some discrepancies in the analytical and experimental curvature distribution plots at the small strain level. This might have been caused by the approximation of the soil profile in the analysis and also from the approximation of initial shear modulus of soil from the N-SPT.

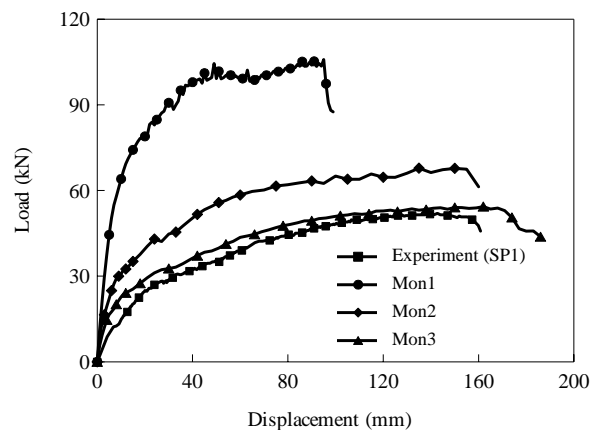


Figure 16. Load-displacement curves from experiment and 3D finite element analysis.

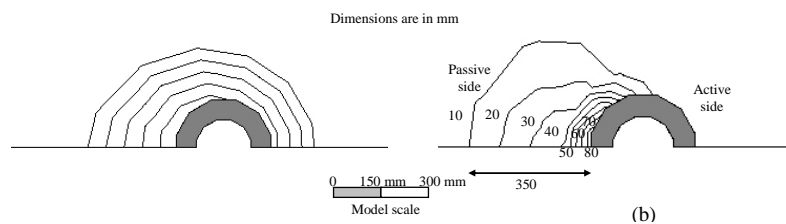


Figure 17. Contours of horizontal soil surface displacements (a) Mon1 and (b) Mon2.

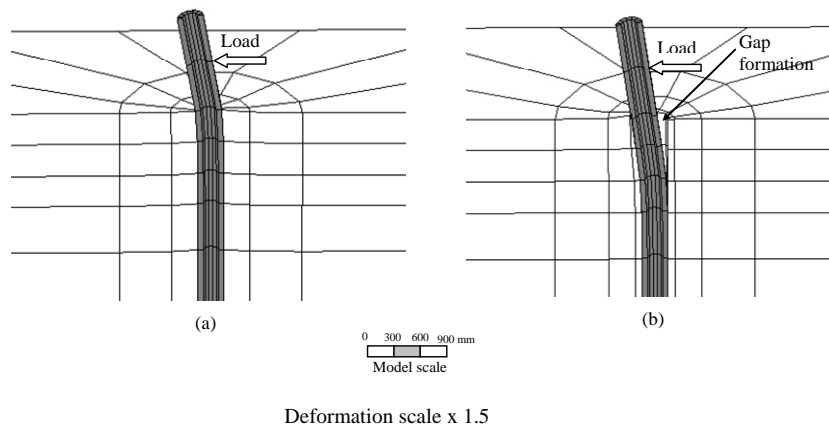


Figure 18. Deflected pile shape and soil deformation (a) without interface element (Mon1) and (b) with interface element (Mon2).

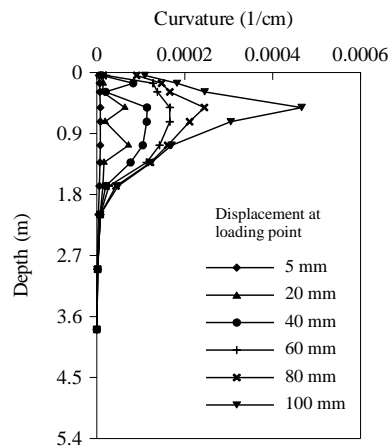


Figure 19. Curvature distribution along pile shaft for case Mon3.

*Reversed cyclic loading*

In the reversed cyclic loading, case Rev1, where an interface element and the bentonite-cement layer around the pile is considered while stiffness degradation is not considered, the analysis overestimates the lateral capacity of the pile (Figure 20a).

In case Rev2, a stiffness degradation factor ( $K_S$ ) of 0.2 was considered parametrically, as shown in Figure 15. Here, the shear stiffness of the soil after the peak strain level of 1% was degraded by 80% following the experimental observation by Thiers and Seed [20]. For a stiffness degradation factor of 0.2, the analytical results tend to agree with the experimental results (Figure 20b). This shows that the degradation in soil stiffness due to reversed cyclic loading is as high as 80% and implies that if the degradation in soil stiffness is ignored, the analytical results highly overestimate the lateral capacity of the piles under reversed cyclic loading.

Figure 21 shows the curvature profile along the depth of the pile for case Rev2. The location of maximum curvature is lower compared to that of the monotonic loading case, Mon3. The plastic hinge was formed 1.3 m from ground level for case Rev2, which correlates well with the experimental results.

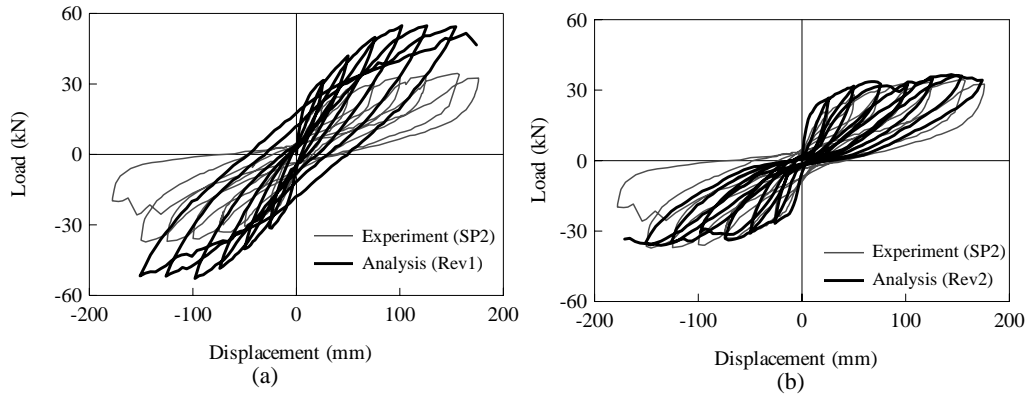


Figure 20. Load-displacement curves from experiment and analysis for reversed cyclic loading.

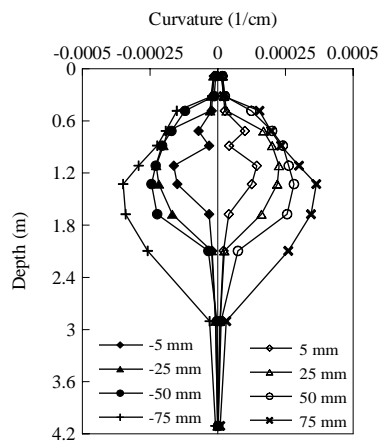


Figure 21. Curvature distribution along pile shaft for case Rev2.

#### 4. CONCLUSIONS

In this study, full-scale monotonic and reversed cyclic lateral loading tests were performed on two instrumented concrete piles embedded into cohesive soil. Three-dimensional finite element analysis was then performed to study the behavior of the experimental specimens. From the experimental study and 3D finite element analysis, the following conclusions can be drawn:

- 1) The study revealed that the formation of a gap between the soil and pile during lateral loading of the pile in cohesive soil has a significant effect on the lateral capacity of the pile. The interface element between the pile and soil used in this study can realistically account for the gap formation.
- 2) The experimental and analytical study clearly exhibited that significant degradation in the lateral load carrying capacity of the pile occurs under reversed cyclic loading compared to monotonic loading. Degradation in reversed cyclic loading is due to the degradation of shear stiffness of the clay due to cyclic loading. The analytical study showed that this degradation could be taken into account by considering the stiffness degradation factor. With an 80% reduction in stiffness of the soil for a shear strain level greater than 1%, the analytical results tend to agree well with the experimental observations. If the degradation in soil stiffness is

ignored, the analytical results greatly overestimate the lateral capacity of the piles under reversed cyclic loading.

3) For pre-boring piles, the presence of a layer of bentonite-cement slurry around the pile has a significant effect on the lateral capacity of the pile. If this bentonite-cement layer is not considered in the analysis, the lateral capacity of the pile is overestimated. Hence, for modeling pre-boring piles, the bentonite-cement layer should be taken into consideration.

#### REFERENCES

1. Mylonakis G, Gazetas G. Seismic soil-structure interaction: beneficial or detrimental? *Journal of Earthquake Engineering* 2000; **4**(3): 277-301.
2. Mylonakis G, Gazetas G, Nikolaou S, Michaelides O. The role of soil on the collapse of 18 piers of the Hanshin Expressway in the Kobe Earthquake. *Proceedings of the 12th World Conference on Earthquake Engineering*, Auckland, New Zealand, 2000. Paper no. 1074.
3. Miyamoto Y. Pile response during earthquake and performance evaluation of pile foundation. *Proceedings of the second UNJR Workshop on Soil Structure Interaction*, Tsukuba, Japan, 2001. Paper no. B-6.
4. Japan Society of Civil Engineers. *Standard Specifications for Concrete Structures – 2002: Seismic Performance Verification*. JSCE Guidelines for Concrete No. 5, 2005.
5. Allen L, Reese L. Small scale tests for the determination of p-y curves in layered soils. *Proc. Of 12<sup>th</sup> Offshore Technology Conference*, 1980. Vol. 1, Paper no. OTC 3747, pp. 109-116.
6. Poulos H G, Chen L T, Hull T S, 1995. Model tests on single piles subjected to lateral soil movement. *Soils and Foundations, Japanese Geotechnical Society* 1995; **35**(4):85-92.
7. Maki T, Mutsuyoshi H. Response behavior of RC piles under severe earthquake. *Proc. of the 12th World Conf. on Earthquake Engineering*, Auckland, New Zealand, 2000. Paper no. 1245.
8. Matlock H. Correlations for design of laterally loaded piles in soft clay. *Proceedings of Offshore Technology Conference*, Dallas, Texas, 1970. Paper no. OTC1204, pp. 577-594.
9. Reese LC. Lateral loading of deep foundations in stiff clay. *Journal of the Geotechnical Engineering Division, Proceedings of the American Society of Civil Engineers* 1975; **101**(GT7): 633-649.
10. Chai Y, Hutchinson C. Flexural strength and ductility of extended pile-shafts II: Experimental study. *Journal of Structural Engineering, American Society of Civil Engineers* 2002; **128**(5): 595-601.
11. Pender MJ, Pranjoto S. Gapping effects during cyclic lateral loading of piles in clay. *Proceedings of the 11th World Conference on Earthquake Engineering*, Acapulco, Mexico, 1996. Paper no. 1007.
12. Trochanis AM, Bielak J, Christiano P. Three-dimensional nonlinear study of piles. *Journal of Geotechnical Engineering* 1991; **117**(3):429-447.
13. Wakai, A, Gose S, Ugai K. 3-D elasto-plastic finite element analysis of pile foundations subjected to lateral loading. *Soils and Foundations, Japanese Geotechnical Society* 1999; **39**(1): 97-111.
14. Kimura M, Zhang F. Seismic evaluations of pile foundations with three different methods based on three-dimensional elasto-plastic finite element analysis. *Soils and Foundations, Japanese Geotechnical Society* 2000; **40**(5):113-132.
15. Maki T, Mutsuyoshi H. Seismic behavior of reinforced concrete piles under ground. *Journal of Advanced Concrete Technology*, Japan Concrete Institute 2004; **2**(1):37-47.
16. Standard method for lateral loading test for a pile. *Japanese Society of Foundation Engineering* 1983. JSF Standard: T 32-83.

17. Maekawa K, Pimanmas A, Okamura H. *Nonlinear Mechanics of Reinforced Concrete*. Spon Press, New York, 2003.
18. Kato B. Mechanical properties of steel under load cycles idealizing seismic action. *Bulletin D' Information CEB, AICAP-CEB Symposium*, Rome, 1979, No. 131, pp. 7-27.
19. Ohsaki Y. Some notes on Masing's law and non-linear response of soil deposits. *Journal of the Faculty of Engineering, The University of Tokyo* 1980; **35**(4):513-536.
20. Thiers GR, Seed HB. Cyclic stress-strain characteristics of clay. *Journal of the Soil Mechanics and Foundation Division, Proceedings of the American Society of Civil Engineers* 1968; **94**(SM2):555-569
21. Castro G, Christian JT. Shear strength of soils and cyclic loading. *Journal of the Geotechnical Engineering Division, Proceedings of the American Society of Civil Engineers* 1976; **2**(GT9): 887-894.
22. Gerolymos N, Gazetas G. Constitutive model for 1-D cyclic soil behavior applied to seismic analysis of layered deposits. *Soils and Foundations, Japanese Geotechnical Society* 2005; **45**(3): 147-159.